27th ABCM International Congress of Mechanical Engineering
December 04-08, 2023, Florianópolis-SC, Brazil

COBEM2023-0766
COMPARISON OF ENERGETIC MODEL APPLIED TO DESALINATION UNIT WITH MULTIPLES EFFECTS

Erick Breno Azevedo dos Santos
Eduardo José Cidade Cavalcanti
Universidade Federal do Rio Grande do Norte, 59072-970, Natal/RN, Brasil
erickbrenoazevedo@gmail.com
educanti@gmail.com

Abstract. *In the past years, the phenomenon of El niño is causing drought in some regions and heavy rains in others, intensifying the demand for fresh water in industrial activities, agriculture and domestic use. The fresh water has become a scarce resource in some locations, and desalination has gained importance as a sustainable option for solving the problem. There are several energy sources used in desalination plants and equipment. The main problem is the high cost of operation, resulting in a more expensive product than the traditional methods used for potable water production. The use of cogeneration with desalination plants is a very effective solution to increase the performance of the desalination process. This system has shown higher thermodynamic efficiency when compared to isolated processes, due to it allows the use of waste thermal energy associated to with high discharge temperature of exhausted gases. Aligned with this method, the use of multi-effect evaporators coupled with steam thermocompressors increases the efficiency of thermal desalination. The present study evaluated a gas turbine electric power generation system with capacity of 40 MW coupled to a multi-effect thermal distillation unit with 6 effects driven by a steam thermocompressor (MED-TVC). The process is modeled using mass and energy balances. A model in literature uses the specific heat constant between the mass flow rate of input and output of brine. The effect of boiling point elevation (BPE) due to salinity of the water was considered. The research has developed a thermal model based on the enthalpy of the saline solution at each mass flow. The models were compared. The power cycle, natural gas combustion and water desalination process were evaluated by energy analysis. The data of base model has a daily production of 13,112 m^3 of desalinated water for 17.81 kg/s of motive steam, resulting in a Gain Output Ratio (GOR) of 8.52.*

Keywords: *Energy recovery, desalination, gas turbine, cogeneration, multi-effect distillation*

1. INTRODUCTION

The water crisis in Brazil has reached a critical stage in recent years, being further aggravated by the scarcity of drinking water in several regions. As a result of the problem, around 35 million Brazilians do not have access to potable water, according to a report by the Instituto Trata Brasil (2021). The problem of water scarcity is not exclusive to Brazil, since a quarter of humanity suffers from an inadequate supply of water (Eltawil et al., 2009). Given this scenario, researches involving analysis, planning and obtaining technologies in order to solve this problem are important. The surface area of the earth is composed of more than two-thirds of water, where 97% of the water is salt water and the rest is fresh water, and less than 1% of this fresh water is available for human production (Mirzaei et al., 2019). There are some current ways to deal with the problem of fresh water scarcity in the world and the desalination is one of them. The desalination removes excess salts in the water and becomes it heathy for human consumption. Currently, several desalination methods are being applied, with emphasis on reverse osmosis, multi-effect distillation and freezing. Desalination processes will be an even stronger trend in the coming years, mainly due to the population increase in underdeveloped countries (United Nations, 2015) and climate change, generating, respectively, an increase in the demand for drinking water and a decrease in the percentage of fresh water available.

However, despite significant efforts, the specific consumption of energy for water production when compared to conventional methods, which work with the treatment of water from rivers, lakes or groundwater, is still very high. Figure 1 shows the comparison of specific consumption for some methods and technologies under development used in desalination according to data published by Jamil et al. (2021). The minimum energy expenditure required to carry out the desalination separation is estimated at 0.72 kWh/m³ for a typical seawater salinity of 35 g/kg at 25°C (Lienhard et al., 2017). The results suggest that current technologies are not optimized enough and operate efficiently far from their thermodynamic limit. Therefore, there is a significant discrepancy that can be reduced with research on energy improvement of existing desalination systems (Jamil and Zubair, 2017).

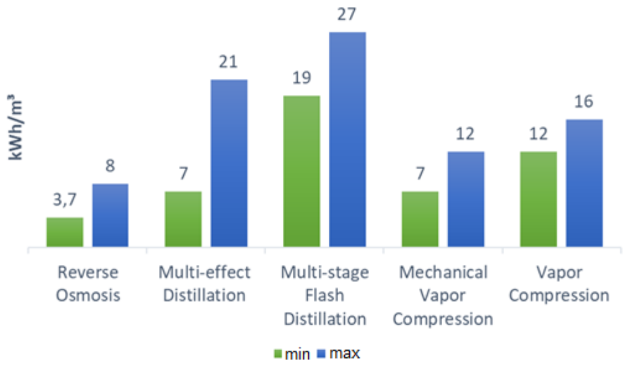

Figure 1. Energy consumption per volume of desalinated water production.

The thermal processes of desalination are based on the difference in the evaporation temperature of water and salts, with the partial separation of the more volatile one occurring and forming a liquid phase and a gaseous phase inside the evaporator. For the process to occur, resources in the form of heat from the burning of a fossil fuel are generally required (Fiorenza et al., 2003) however, new systems are also using renewable sources.

Multi-effect distillation with thermal vapor compression (MED-TVC) is gaining more interest compared to other thermal desalination processes. This system plays an important role in the production of fresh water in dry regions of the world and, mainly, in Arabia, one of the main references on the development of desalination technologies (Al-Mutaz and Wazeer, 2014). Thermal desalination systems can be integrated into electrical power generation plants. This possibility uses the waste heat from the power plant as input heat to the system and increases the total efficiency of the thermodynamic cycle. Other alternative systems may use more than one form of motive energy input, as such as fossil fuel and solar energy. Moreover, power cycles are already widely used in various engineering applications, whether to obtain electrical or mechanical power. In both applications, the cycles have a high value of rejected heat, called process heat and this heat can be used for other purposes through cogeneration (Çengel and Boles, 2013). The use of process heat as energy source of a desalination plant using a multistage evaporator can reduce the operating costs of the system. In this way, the thermal energy that would naturally be rejected would be contributing to the distillation of seawater.

Researches in the area shows that the use of a thermocompressor before entering the extracted steam into the first stage of the system plays an important role in the multi-effect evaporator. It reduces energy consumption and increases system efficiency, although energy consumption can be significantly influenced by the geometry and operating conditions of the thermocompressor (Al-Mutaz and Wazeer, 2014).

2. SYSTEM DESCRIPTION

A multi-effect distillation desalination system with an integrated thermocompressor coupled to a gas turbine plant is considered for the study as shown in Figure 2. The environmental air is drawn the compressor under standard atmospheric conditions and after undergoing compression it flows to the combustion chamber, where the natural gas is burned. The combustion gases expand in the turbine producing power and maintaining a high thermal energy value. The exhausted gases are conducted to the heat recovery exchanger (HRSG). The HRSG is responsible for transferring heat between the flue gases and the motive steam to drive the desalination unit. The pumped water becomes motive steam flows into the HRSG exiting as saturated steam state. The motive steam is then directed to the thermocompressor, reducing its pressure and drawing the steam from the last evaporator (effect). Finally, the steam flows to the desalination unit with six effects, where all pressures are reduced. Inside the evaporator, the salt water is separated in desalinated steam and brine. The technical conditions and input variables are present in Table 1 and are adapted from the study considered by Ahmadi et al. (2020).

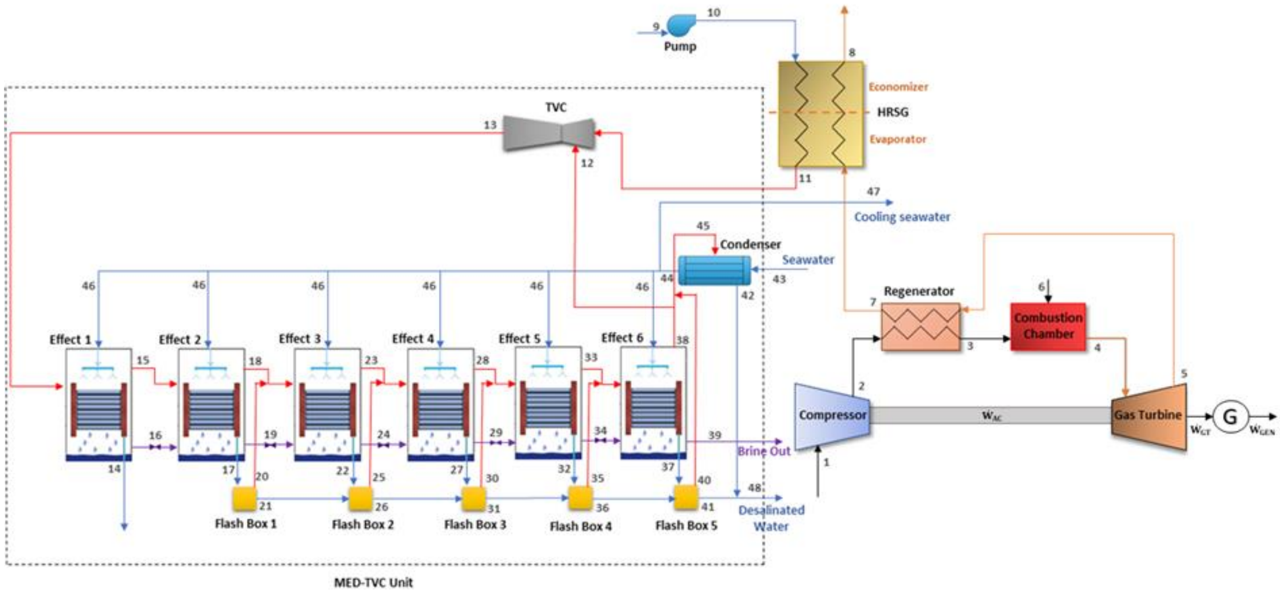

Figure 2. Model schematic diagram.

Table 1. Model input parameters.

Parameter	Value
Ambient temperature	25 °C
Ambient pressure	101 kPa
Compressor isentropic efficiency	0.85
Regenerator efficiency	0.60
Turbine isentropic efficiency	0.89
Pump isentropic efficiency	0.70
Compressor pressure ratio	10
Electric generator power	40 MW
Combustion gases mass flow	2,26 kg/s
Turbine input temperature	1100 °C
Combustion chamber pressure loss	2%
Combustion chamber heat loss	2%
Fuel input pressure	460 kPa
Water input pressure in HRSG	1000 kPa
TVC compression ratio	2.9
Pressure on the 1° effect	27.37 kPa
Pressure on the 2° effect	23.51 kPa
Pressure on the 3° effect	20.13 kPa
Pressure on the 4° effect	17.17 kPa
Pressure on the 5° effect	14.59 kPa
Pressure on the 6° effect	12.35 kPa
Seawater salinity	36,000 ppm

The percentage composition of natural gas is shown in Table 2. The values of the lower heating value (LHV) of each component were obtained as reported by Baghernejad and Yaghoubi (2011).

Table 2. Composition of natural gas.

Component	Volume (%)	Mass (%)	LHV (kJ/kg)
CH_4	88.82	80.33	50,000
C_2H_6	8.41	14.26	47,525
C_3H_8	0.55	1.37	46,390
N_2	1.62	2.56	-
CO_2	0.60	1.48	-
Total	100.00	100.00	47,574

3. ENERGY MODELING OF THE SYSTEM

3.1 Brayton cycle and combustion

The composition of atmospheric air is assumed as a mixture of 23.2% oxygen and 76.8% nitrogen of mass percentage. The enthalpy (h) of each point was obtained by multiplying the mass percentage of each gas component by the intensive property in the temperature and/or pressure condition at the according specified point. The gases were considered ideal.

$$h_i = \sum x_i \cdot h_{i,T} \tag{1}$$

The complete combustion reaction is expressed in Eq. 2 and takes into account mole fractions for 1 kmol of fuel. The values used can be obtained through the equivalence ratio between the volumetric percentage of the gas composition and its molar composition.

$$\begin{aligned} y_{CH_4} \cdot CH_4 + y_{C_2H_6} \cdot C_2H_6 + y_{C_3H_8} \cdot C_3H_8 + y_{N_2} \cdot N_2 + y_{CO_2} \cdot CO_2 + \varphi \cdot \lambda \cdot (O_2 + 3{,}76N_2) \\ \rightarrow n_{CO_2} \cdot CO_2 + n_{H_2O} \cdot H_2O + (\varphi - 1) \cdot \lambda \cdot O_2 + \varphi \cdot n_{N_2} \cdot N_2 \end{aligned} \tag{2}$$

Where λ is the stoichiometric requirement of oxygen. φ is the theoretical air used at air excess. The theoretical air is higher than one, meaning that there is a combustion reaction with excess air. This is necessary to limit the temperature at the turbine input due to the metallurgical temperature limit of the materials.

The air fuel ratio (A/F) can be calculated at Eq. 3, where the molar mass (M) of the fuel is relative to the contribution of the molar mass of each natural gas component.

$$A/F = \frac{\varphi \cdot \lambda \cdot (x_{O_2} + 3{,}76 \cdot x_{N_2})}{M_{fuel}} \tag{3}$$

The energy balance or the first law of thermodynamics is applied with chemical reactions. The corresponding enthalpies of formation of each compound and the losses related to combustion are considered as follows eq. (4).

$$\sum h_{reagents} = \sum h_{product} + \dot{Q}_{loss} \tag{4}$$

The efficiency of combustion chamber (η_{cc}) is 98%, thereby the rate of heat loss in the combustion chamber ($\dot{Q}_{loss}$) represents 2% of the LHV based on the data in Table 2 according to eq. (5).

$$\dot{Q}_{loss} = \dot{m}_{fuel} \cdot LHV.(1 - \eta_{cc}) \tag{5}$$

The efficiency of the Brayton cycle is calculated by net power and rate heat produced at combustion according to Eq. (6).

$$\eta_{cycle} = \frac{\dot{W}_{turbine} - \dot{W}_{compressor}}{\dot{m}_{fuel} \cdot LHV} \tag{6}$$

3.2 Heat recovery steam generation (HRSG)

The HRSG is composed of an economizer and evaporator. In economizer, the water used as motive steam in the desalination unit exchanges sensible heat with the combustion gases, and in the evaporator, the water exchanges latent heat, leaving the HRSG as saturated steam.

There are two parameters at the sizing of HRSG called: Pinch point and approach point. The pinch point (PP) is defined as the temperature difference between the hot fluid (exhaust gases) and the cool fluid (saturated steam). The approach point (AP) is defined as the temperature difference between the saturated steam and the condensate liquid leaving the economizer (Matelli, 2008). The approach point was assumed zero in this work. It is recommended that the exhaust gas temperature be above 130 °C at the output of the HRSG to avoid acid condensation and corrosion problems.

3.3 Thermo vapor compressor (TVC)

The TVC is responsible for reduce the pressure into evaporators. It mixes the motive steam with a portion of the steam produced in the last stage in the desalination unit, which is called entrained steam. In this way, it is possible to reduce the motive steam pressure practically without losses. The steam produced at the output has a high thermal energy for subsequent heat transfer in the first stage of the evaporator of the desalination unit.

There are three main parameters in the TVC: the compression ratio, the expansion ratio and the entrainment ratio. The compression ratio (C_r) is given by the ratio of the pressure at the output of the TVC and the pressure in the last stage of the evaporator as follows at Eq. 7. It is defined as an input parameter as shown in Table 1. The expansion ratio (E_r) is given by the ratio between the motive steam pressure and the entrained steam pressure according to Eq. 8. The entrainment ratio (R_a) is the ratio of mass flow rate between the motive steam and entrained vapor. There are several calculation methods (Al-Mutaz and Wazeer, 2014) to entrainment ratio. The assumed relation in the work was developed by the empirical method according to El-dessouky and Ettouny's (2002) as follows in Eq. 9 and 10.

$$C_r = \frac{P_s}{P_{ev}} \tag{7}$$

$$E_r = \frac{P_m}{P_{ev}} \tag{8}$$

$$R_a = 0{,}235 \cdot \frac{{P_s}^{1{,}19}}{{P_{ev}}^{1{,}04}} \cdot {E_r}^{0{,}015} \tag{9}$$

$$R_a = \frac{\dot{m}_m}{\dot{m}_{ev}} \tag{10}$$

Where P_s is pressure of compressed vapor (P_{13}), P_{ev} is entrained vapor pressure (P_{12}), Pm is pressure of motive steam (P_{11}), $\dot{m}_m$ is motive steam flow rate ($\dot{m}_{11}$) and $\dot{m}_{ev}$ is entrained vapor flow rate ($\dot{m}_{12}$).

3.4 Multi-effect distillation (MED) unit

The thermal desalination unit is composed of six evaporator effects, five flash chambers and a condenser. The first effect, commonly called pre-evaporator, is the only effect driven by the compressed vapor produced in the TVC. In the following effects, the heat exchange is performed between the brine flow and the steam from the previous stage. All pressures are lower than to the atmospheric pressure. The pressures in each stage are design parameters and are listed in Table 1.

According to Ahmadi et al. (2020), the supplied seawater temperature (T_{46}) was defined at 45°C, and it was considered that the MED system does not exchange heat with the external environment. Also, the salinity of the brine rejected in the last effect is limited to 70000 ppm due to environmental concerns. The mass and chemical species balances were conducted for all desalination effects.

The brine temperature (T_i) is higher than to the water saturation temperature ($T_{sat,water}$) due to the salinity effect. The increase of temperature is called the boiling point elevation (BPE), which is obtained according to Al-Mutaz and Wazeer (2014). The brine temperature is evaluated by the water saturation temperature ($T_{sat,water}$) plus the boiling point elevation (BPE) as shown in Eq. 11.

$$T_i = T_{sat,water} + BPE \tag{11}$$

BPE is calculated using the constants B and C, by Eq.12.

$$BPE = X_i \cdot [B + C \cdot (X_i)] \cdot 10^{-3} \tag{12}$$

$$B = [6.71 + (6.34 \cdot 10^{-2} \cdot T_i) + (9.74 \cdot 10^{-5} \cdot {T_i}^2)] \cdot 10^{-3} \quad (13)$$

$$C = [22.238 + (9.59 \cdot 10^{-3} \cdot T_i) + (9.42 \cdot 10^{-5} \cdot {T_i}^2)] \cdot 10^{-8} \quad (14)$$

The specific heat (c_p) of salt water in (kJ/kg.K) is function of temperature and salinity, and should be evaluated at each effect for output brine and input seawater flows according to Al-Mutaz and Wazeer (2014) in Eq. 15.

$$c_p = [a + (b \cdot T_i) + (c \cdot {T_i}^2) + (d \cdot {T_i}^3)] \cdot 10^{-3} \quad (15)$$

$$a = 4206,8 - (6,6197 \cdot S) + (1,2288 \cdot 10^{-3} \cdot S^2) \quad (16)$$

$$b = -1,1262 + (5,4178 \cdot 10^{-2} \cdot S) + (2,2719 \cdot 10^{-4} \cdot S^2) \quad (17)$$

$$c = 1,2026 \cdot 10^{-2} - (5,3566 \cdot 10^{-4} \cdot S) + (1,8906 \cdot 10^{-6} \cdot S^2) \quad (18)$$

$$d = 6,8777 \cdot 10^{-7} - (1,517 \cdot 10^{-6} \cdot S) + (4,4268 \cdot 10^{-9} \cdot S^2) \quad (19)$$

Where T is the temperature in Celsius. S is the water salinity in (g/kg) evaluated by the mass salinity of water (x) in ppm at Eq. 25.

$$S = \frac{X_i}{1000} \quad (20)$$

The simplified energy model used in literature considered the same specific heat for input seawater and output brine. The energy balance in first effect in Figure 1 according to Ahmadi et al. (2020) is shown in Eq. 21.

$$\dot{m}_{15}.L_{15} = \dot{m}_{13}.L_{13} - \dot{m}_{46}.c_p.(T_{16} - T_{46}) \quad (21)$$

Where L is the latent heat of steam.

The Eq. 21 not consider the sensible heat of flows 13 and 15 and doesn´t distingue the specific heat of flows 16 and 46 that have different temperature and salinity. The energy balances of next effects include the input of brine solution from previous effect.

The energy model used in this research works with the enthalpy which has no simplification as the model. The enthalpies of saline water are defined based on the references (h_0) and (T_0) using cp according to Eq. 22. The reference adopted herein defines that enthalpy of water in the saturated liquid state (h_0) is zero when temperature (T_0) is 0.01 °C.

$$h_i = h_0 + c_p(T_i - T_0) \quad (22)$$

Flash chamber increases the produced steam for next effect. It reduces the pressure of condensed steam from the previous effect to the pressure in the next effect. In this equipment, the pressure of condensed liquid is reduced and saturated steam is produced and the remain keep as saturated liquid. The produced steam goes the next effect increasing the heat exchange. This configuration allows improve the use of the thermal energy of the desalinated condensate, as its pressure is higher than to next evaporator.

The mass flow rate of seawater feed ($\dot{m}_{46}$) is defined by the energy balance in the condenser where heat this flow at temperature T_{46} , following Ahmadi et al. (2020). Despite being initially fixed, T_{46} affects the performance of the MED-TVC system.

The desalination unit produces the desalinated water ($\dot{m}_{48}$) and brine ($\dot{m}_{39}$). The performance of a desalination system can be assessed by the gain output ratio (GOR), being the ratio of desalinated water production rate ($\dot{m}_t$), which is equal to $\dot{m}_{48}$, and the motive steam rate ($\dot{m}_m$), which is equal to $\dot{m}_{11}$ as expressed by Eq. 23,

$$GOR = \frac{\dot{m}_t}{\dot{m}_m} \quad (23)$$

4. RESULTS AND DISCUSSION

In this section, the results of the thermodynamic modeling are presented, which include the thermal efficiencies of the gas power cycle, the energy analysis of the system, the productive capacity of the desalination unit. Furthermore, a comparison of the enthalpy model with the constant cp model performed by Ahmadi et al. (2020).

4.1 Combustion and gas power cycle

With the established conditions, the natural gas combustion parameters such as: the stoichiometric requirement (λ), the excess air ($\varphi - 1$), which were developed in Eq. 2 and Eq. 3, the air mass rate ($\dot{m}_{air}$), and the real combustion heat rate ($Q_{in,real}$) are shown in Table 3.

Table 3. Results of combustion process.

$\boldsymbol{\lambda}$	$\boldsymbol{\varphi - 1}$	$\dot{\mathbf{m}}_{\mathbf{air}}$	$\mathbf{Q}_{\mathbf{in,real}}$
2.098	2.59	133.6 kg/s	105.368 MW

For net power of 40 MW, the mass flow rate of exhausted gases from turbine is calculated as 135.8 kg/s, and the fuel air ratio (A/F) of the combustion is 59.09 kg/kg. Ahmadi et al. (2020) has value of mass flow ratio of 113.87 kg/s with air fuel ratio of 50.38 kg/kg. This difference is justified by the composition of the fuel. In work of Ahmadi et al. (2020), pure methane (CH_4) was used as an approximation in natural gas and the present work better explored the composition of natural gas as shown in table 2.

With the net power of the cycle fixed at 40 MW, the power produced by the turbine is 85.9 MW and the power consumed by the compressor is 44.6 MW. Thus, it implies a work consumption ratio of 51.86%, that is, about half of the work is consumed by the compressor. The efficiency of the Brayton cycle is 37.2% according to eq. (6). In work of Ahmadi et al. (2020), this value of efficiency was 35.3%. The efficiency is higher, due the regenerator presence in the present work, which preheats the compressed air before the combustor. The regenerator reduces the temperature of the combustion gases at the input of the HRSG. This input temperature is 448.7 °C, while in the study by Ahmadi et al. (2020), it is 580.8 °C, because they have not regenerator.

4.2 MED unit

The input seawater salinity is adopted as 36,000 ppm and the output brine salinity is 70,000 ppm, according to Ahmadi et al. (2020). Both turbines have the same net power. The motive steam mass flow rate is 17.81 kg/s, greater than that of Ahmadi et al. (2020) (14 kg/s).

A comparison between the constant cp model of Ahmadi et al. (2020) and the enthalpy model employed here was evaluated based on the salinity in each effect. Table 4 shows the relative difference of salinity of the output brine between the models.

Table 4. Output brine salinity at each evaporator effect.

Component	**Salinity (ppm)**		
	This study	**Ahmadi et al. (2020)**	**Relative difference**
Effect 1	76,481	76,829	0.453%
Effect 2	73,893	74,296	0.542%
Effect 3	72,021	72,501	0.662%
Effect 4	70,787	71,231	0.623%
Effect 5	70,126	70,411	0.405%
Effect 6	70,000	70,000	0.000%

The salinity of output brine for effects 1-5 are slightly lower than Ahmadi et al. (2020). The enthalpy of the brine solution considers the energy at any state from the same dead state as 0°C and atmospheric pressure. The specific enthalpy of input seawater is different from that of output brine, due to the different salinities. However, the specific heat model considers only the variation of enthalpy with same salinity and temperature. The enthalpy model takes into account enthalpy variation with salinity and temperature between the brine flows. The relative difference between the models is slight.

Table 5 shows the results of the energy balance at each point of the cogeneration plant.

Table 5. State properties of cogeneration plant

State	T (°C)	P (kPa)	ṁ (kg/s)	State	T (°C)	P (kPa)	ṁ (kg/s)
1	25.0	101.00	133.60	25	60.2	20.13	0.35
2	341.8	1010.00	133.60	26	60.2	20.13	57.88
3	488.2	1010.00	133.60	27	60.2	20.13	27.31
4	1100.0	989.80	135.80	28	56.8	17.17	26.42
5	585.9	101.00	135.80	29	58.7	17.17	115.50
6	25.0	460.00	2.26	30	56.8	17.17	0.51
7	448.7	101.00	135.80	31	56.8	17.17	84.68
8	130.0	101.00	135.80	32	56.8	17.17	26.93
9	25.0	101.00	17.81	33	53.4	14.59	26.54
10	25.1	1000.00	17.81	34	55.3	14.59	145.70
11	179.9	1000.00	17.81	35	53.4	14.59	0.67
12	50.0	12.35	13.71	36	53.4	14.59	110.90
13	111.7	35.82	31.51	37	53.4	14.59	27.21
14	73.2	35.82	31.51	38	50.0	12.35	27.31
15	67.0	27.37	30.05	39	51.8	12.35	175.20
16	69.2	27.37	26.72	40	50.0	12.35	0.82
17	67.0	27.37	30.05	41	50.0	12.35	137.30
18	63.6	23.51	28.18	42	50.0	12.35	14.43
19	65.7	23.51	55.32	43	25.0	101.00	428.40
20	63.6	23.51	0.18	44	45.0	101.00	428.40
21	63.6	23.51	29.87	45	50.0	12.35	14.43
22	63.6	23.51	28.36	46	45.0	101.00	56.78
23	60.2	20.13	26.96	47	45.0	101.00	87.77
24	62.2	20.13	85.14	48	50.0	12.35	151.80

The mass rate of desalinated water produced in each stage can be verified at points 15, 18, 23, 28, 33, 38. The total mass rate of produced water is 151.80 kg/s at temperature of 50°C. The mass rate of rejected brine is 175.20 kg/s at point 39 with a slightly higher temperature of 51.8 °C. In this condition, it results in 1.15 kg of brine produced for 1 kg of desalinated water.

The mass flow rate of input seawater into each effect is constant at point 46 and equal to 56,78 kg/s. The motive steam flow rate at point 11 is 17.81 kg/s and ejector output temperature at point 13 is 111.7 °C. These parameters at work of Ahmadi et al. (2020) were similar as: The mass flow rate of input seawater was 55.47 kg/s; the motive steam flow rate was 14.00 kg/s and the ejector output temperature was 73°C. The last temperature has a significant difference. This fact is related with a configuration of thermal vapor compression (TVC). It receives at the input, the motive steam at high pressure (1000 kPa) and high saturation temperature (179.9 °C) and the entrained steam at low pressure (12.35 kPa) at a temperature of 50 °C. At the output, steam is delivered at low pressure as 35.82 kPa with a high temperature (111.7 °C). This steam state has a higher thermal energy to carry out a latent heat transfer in the first effect. If the TVC process was isentropic the final temperature of ejector output will be 112,9 °C. However, this value at Ahmadi et al. (2020) was 73 °C. This low value can occur if there is an intense heat loss to the environmental, which has no sense. The presence of a desuperheater is able to produce this lowest temperature of steam by the injection of water into a steam flow.

Other comparison can be evaluated consider the capacity and performance of desalinated water. In the present work, which uses the enthalpy model, the desalinated water flow is 13,122 m^3/day with the parameter GOR calculated by Eq. 23 is (151.8/17.81=8.52). In Ahmadi et al. (2020), its value was 12,294 m^3/day with the parameter GOR of (139.3/14=9.95). The production of desalinated water from the enthalpy model is higher. This fact can be justified by the higher thermal energy of output ejector steam. The performance based on GOR is lower, due to the higher motive steam mass flow rate produced into gas turbine system, which is 17.81 kg/s in comparison of value of Ahmadi et al. (2020) as 14 kg/s. The motive steam mass rate of the present study was 27% higher than the work by Ahmadi et al. (2020). However, the difference in the production of desalinated water was only 6.7%.

The values of boiling point elevation (BPE) of output brine flow at each evaporator are shown in Table 6.

Table 6. BPE in each effect

Component	BPE (°C)	Component	BPE (°C)
Effect 1	2.251	Effect 4	1.921
Effect 2	2.105	Effect 5	1.871
Effect 3	1.998	Effect 6	1.844

The value of BPE changes from 2.251 to 1.844 °C from point 16 to 39 at output of evaporators. It is important to note that the salinity changed from 76,481 to 70,000 ppm. As the salinity increases, the BPE increases according to Eq. 12. This highlights the importance of using different enthalpy values for each brine flow.

In order to compare the models with the same input variables, as such as, the motive steam flow rate of 14 kg/s, the TVC output temperature of 73°C and the feed seawater temperature of 45°C, the performance was evaluated. The heat transfer into first evaporator at steam side is equal.

The capacity of distillated water of 9,709 m^3/day is lower than to Ahmadi et al. (2020) of 12,294 m^3/day. This results can be explained since the enthalpy mode takes into account the sensible heat of sea water and brine input flows and the effect of temperature and salt concentrations of brines as discussed in Eq. 22. The specific heat model not considers these differences of seawater input and brine output, and, thus, it overestimates the mass flow rate of desalinated water. The mass flow rate of input seawater of 50.82 kg/s in point 46 is lower than to Ahmadi et al. (2020) of 55.47 kg/s. Even with the same heat transfer into first evaporator, the side of salt water has lower capacity to produce distillated water at enthalpy model. Additional, the performance of distillation unit based on GOR of 8.027 is lower than to specific heat model with GOR of 9.95. And the salinity changes from 64,823 ppm in first effect to 60,388 ppm in last effect with lower values due to low mass flow rate of input seawater.

5. CONCLUSION

The work evaluated the thermodynamic conditions of a cogeneration plant composed of a gas power cycle integrated with a desalination unit with 6 effects and its auxiliary components. Some input parameters of the project were defined according to literature data. The enthalpy of each flow of the desalination unit is considered, according to its salt concentration and temperature. The enthalpy model provides more accurate results mainly in flow rate of desalinated water and brine.

The gas turbine produced 40 MW, and the mass flow rate of motive steam is 2.26 kg/s. The mass flow rate of desalinated water is 151.80 kg/s, the mass flow rate of seawater into each effect is 56.78 kg/s, and the mass flow rate of discharged brine is 175.20 kg/s.

The results showed the potential for the production of distilled water by the thermal desalination process, which enables alternative means for the production of water for human consumption.

For future work, it is necessary to use optimization methods to define the ideal number of stages, as well as to evaluate the exergy and economic aspects of the cogeneration system. In addition, it is possible to analyze the environmental impacts of flue gases, in a more robust model, and of the rejected brine.

6. ACKNOWLEDGEMENTS

The development of this article was possible thanks to the support of the National Council for Scientific and Technological Development (CNPq) productivity grant No. 306471/2022-1 and Master scholarship. And CAPES for financial support with travel to congress.

7. REFERENCES

Ahmadi, P., Khanmohammadib, S., Musharavatic, F., Afrand M., 2020, Development, evaluation, and multi-objective optimization of a multi-effect desalination unit integrated with a gas turbine plant, *Applied Thermal Engineering*, Vol. 176. pp. 115414.

Al-Mutaz, S. I., I. Wazeer, 2014, Development of a steady-state mathematical model for MEE-TVC desalination plants, *Desalination*. Vol. 351, pp. 9 – 18.

Baghernejad, A., Yaghoubi, M, 2011, Multi-objective exergoeconomic optimization of an Integrated Solar Combined Cycle System using evolutionary algorithms, *Internacional Journal of Energy Research*, Vol. 35, pp. 601 – 615.

Çengel, Y. A., Boles, Michael A., 2013. *Thermodynamics: An Engineering Approach*, 7th Edition. Editora McGraw Hill.

El-Dessouky, H.T, Ettouney, H. M, 2002, Fundamentals of salt water. *Desalination*, 1st Edition, Elsevier.

Eltawil, M. A, Zhao, Z, Ligiang, Y., 2009, A review of renewable energy technologies integrated with desalination systems". *Renewable and Sustainable Energy Reviews*, Vol. 13, pp. 2245-2262.

Fiorenza, G., Sharma, V.K., Braccio, G, 2003, Techno-economic evaluation of a solar powered water desalination plant, *Energy Conversion and Management*, Vol. 44, pp. 2217 – 2240.

Instituto Trata Brasil, 2021. Executive Summary, Basic Sanitation Ranking (In Portuguese). https://tratabrasil.org.br/images/estudos/Ranking_saneamento_2021/Resumo_Executivo.pdf. Accessed 15 Sep 2022.

Jamil, M.A., Haseeb, Y., Asad, A., Muhammad, U. F., Noor, U. S., Ben, B. X., Laurent, D., Kim, C. Ng., Muhammad, W. S., 2021, An exergoeconomic and normalized sensitivity based comprehensive investigation of a hybrid power-and-water desalination system, *Sustainable Energy Technologies and Assessments*, Vol. 47, pp. 101463.

Jamil, M. A., Zubair, S. M., 2017, On thermoeconomic analysis of a single-effect mechanical vapor compression desalination system, *Desalination*, Vol. 420, pp. 292-307.

Lienhard J.H., Mistry K.H., Sharqawy M.H., Thiel G.P., 2017, Thermodynamics, Exergy, and Energy Efficiency in Desalination Systems, *Desalination Susteinability*, Chapter 4, pp. 127-206.

Matelli, J. A., 2008. *Knowledge-based systems for designing natural gas cogeneration plants* (In Portuguese). Thesis, Federal University of Santa Catarina.

Mirzaei A., Saghafian B., Mirchi A., Madani K., 2009, The Groundwater–Energy–Food Nexus in Iran's Agricultural Sector: Implications for Water Security, *Water*, Vol. 11, pp. 1835.

United Nation Organization, 2015. *World Population Prospects: The 2015 Revision Summary and Key Findings*. https://population.un.org/wpp/Publications/Files/Key_Findings_WPP_2015.pdf. Accessed 02 Oct 2022.

8. RESPONSIBILITY NOTICE

The authors are the only responsible for the printed material included in this paper.